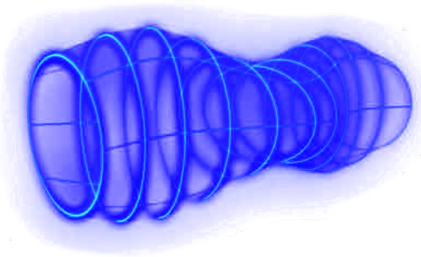

University of Nebraska - Lincoln
Physics & Astronomy

Comprehensive Examination

The Observation of Gravity waves at LIGO

Author:

Caleb Fangmeier

Supervisory Committee:

Dr. Gregory Snow (Chair)
Dr. Christian Binek
Dr. Daniel Claes
Dr. Sebastian Elbaum
Dr. Ilya Kravchenko

Abstract

On September 14, 2015 09:50:45 UTC, the first direct observation of a gravitational wave was made by the Advanced LIGO experiment. The event, deemed GW150914[1], was determined to be caused by the inspiral and subsequent merger of two stellar-mass black holes. Subsequently, on December 26, 2015 03:38:53 UTC another black hole merger event was observed[2]. These two observations confirm the predictions of general relativity in the highly non-linear strong field regime as well as cosmological predictions of the existence of binary black hole systems. Here I discuss the theoretical mechanisms enabling the observation of gravitational waves, the design of the Advanced LIGO detector, the extraction of events from data, and the implications to various cosmological models.

June 1, 2017

Contents

I. Introduction

In 1916, Albert Einstein predicted the existence of gravity waves as a consequence of his theory of general relativity. However, despite a century of experimental effort, direct observation eluded scientists until September 2015 when the Advanced Laser Interferometer Gravitational-Wave Observatory (LIGO) observed a gravity wave resulting from a binary black hole merger.

The structure of this paper is as follows: In Section II I will go through the history of gravitational waves beginning with their first theoretical predictions and continuing through early efforts at direct detection by Weber and others. Section III is a thorough description of the Advanced LIGO detector itself. Section IV describes the data analysis strategies employed to find evidence of gravity waves in the data coming from the detector. Section V describes the two published gravity wave observations made in the first observing run of Advanced LIGO. Section VI Briefly describes some of the implications of the observed events on cosmology. And finally Section VII gives some closing remarks.

II. The History of Gravity Waves

In this section, I give an overview of some of the history of gravity waves from their tumultuous theoretical origins to early efforts at detection.

i. The Existential Question

In 1905 Henri Poincare published "Sur la dynamique d' l'èlectron"[1][3]. In the paper, Poincare described his theory of relativity which based the existence of gravity waves on analogy with the electro-magnetic waves produced by accelerating charges. However, it would take until 1916 for Einstein to publish his Theory of General Relativity[4]. This theory, which was in many ways an extension of his Theory of Special Relativity, viewed gravity not as a force, à la Newton, but instead as a curvature in space-time brought about by the presence of mass and energy. Expressed mathematically, Einstein's field equations can be written in tensor form as

$$R_{\mu\nu} - \frac{1}{2}Rg_{\mu\nu} + \Lambda g_{\mu\nu} = \frac{8\pi G}{c^4}T_{\mu\nu}$$

where $R_{\mu\nu}$ is the Ricci curvature tensor, R is the scalar curvature, $g_{\mu\nu}$ is the metric tensor, Λ is the cosmological constant, G is Newton's gravitational constant, and $T_{\mu\nu}$ is the stress-energy tensor.

[1] On the Dynamics of the Electron

Roughly speaking, the right-hand side of the equation is determined by a distribution of mass and energy and the left-hand side represents the resulting space-time curvature. Unfortunately, although the equation appears relatively simple, both the Ricci tensor and the scalar curvature depend on the metric tensor in a complicated nonlinear manner. As a result, in only a small number of cases with readily exploitable symmetries have the field equations been solved analytically. In fact, it has taken great efforts in the field of Numerical Relativity to be able to obtain the necessary theoretical results for LIGO to know what the signature of various astronomic calamities (e.g. binary black-hole mergers) would look like.

But back in 1916, Einstein was still grappling with his nascent theory and its implications. For example, because there is no such thing as negative mass in General Relativity (in contrast to electro-magnetism where charge comes with positive *and* negative signs), one cannot construct a gravitational dipole or resulting dipole radiation. By 1936, Einstein and his student Nathan Rosen had arrived at the conclusion that gravity waves could not exist in the theory. Indeed, they submitted a paper to the *Physical Review* stating as much. The editor forwarded the paper to the referee, Howard Percy Robertson, who pointed out several flaws in the paper. Einstein, apparently unfamiliar with the peer review process, responded to the criticism.

> *July 27, 1936*
>
> *Dear Sir.*
>
> *"We (Mr. Rosen and I) had sent you our manuscript for publication and had not authorized you to show it to specialists before it is printed. I see no reason to address the-in any case erroneous-comments of your anonymous expert. On the basis of this incident I prefer to publish the paper elsewhere."*
>
> *Respectfully*
>
> *Einstein*
>
> *P.S. Mr. Rosen, who has left for the Soviet Union, has authorized me to represent him in the matter.*

With the departure of Rosen, another young physicist named Leopold Infeld became the new assistant to Einstein. Infeld befriended Robertson and together they confirmed the error in the original Einstein-Rosen submission. Infeld proceeded to point out the error to Einstein who was then obligated to submit a letter to the editor of the *Journal of the Franklin Society* where he had eventually submitted the paper after its rejection by *Physical Review*. The revised paper contained the following conclusion.

> "Rigorous solution for Gravitational cylindrical waves is provided. For convenience of the reader the theory of gravitational waves and their production, known in principle, is presented in the first part of this article. After finding relationships that cast doubt on the existence of gravitational fields rigorous wavelike solutions, we have thoroughly investigated the case of cylindrical gravitational waves. As a result, there are strict solutions and the problem is reduced to conventional cylindrical waves in Euclidean space."

In the end, Einstein came to understand that gravitational waves were a real part of General Relativity. However, it remained to be seen how such waves could be seen in experiment.

ii. Physical Interpretations

Unfortunately for the experimentalist, the coordinate systems commonly employed for calculations in the realm of General Relativity were chosen for reasons of mathematical simplicity, not for easily extracting observables or making comparisons with experiment. In 1956, Felix A. E. Pirani addressed this problem in his paper "On the physical significance of the Riemann tensor"[5]. In his paper, Pirani deduced the effects of space-time curvature to an observer in an inertial frame. Crucially, Pirani showed that particles are oscillated by the passing of a gravity wave.

It is worth pausing here to describe in greater detail the physical nature of gravity waves. First of all, these waves travel at the speed of light, which could be seen as either a direct consequence of General Relativity, or a result of a massless graviton. The stretching and squeezing of space is always and only transverse to the direction of propagation and is invariant under a 180° rotation around the axis of propagation. The waves come in two polarizations, the $+$ polarization, which affects free particles as depicted in Fig. 1, and the $\times$ polarization which is rotated 45° with respect to the $+$ polarization. These waves can be red shifted and gravitationally lensed, just like electro-magnetic waves. However, unlike electro-magnetic waves, they are only negligibly dispersed by interactions with matter[6].

In the year following Pirani's paper, the seminal Chapel Hill conference was held on the campus of the University of North Carolina, and among the many notable attendees were Richard Feynman, Julian Schwinger, and John Wheeler. The conference has organized by the Institute of Field Physics (IOFP), under the patronage of eccentric millionaire Roger W. Babson. Of the many topics covered at the six-day conference, one of the most hotly debated was the question of whether gravity waves were able to carry energy. To

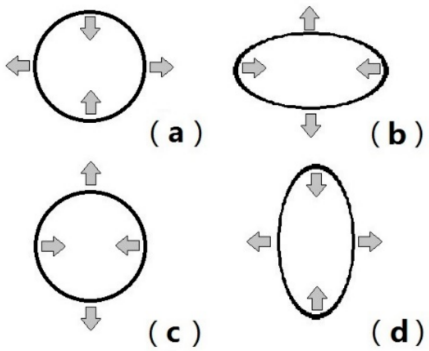

Figure 1: *The effect of a $+$ polarized gravitational wave propagating into the page on a ring of free particles. Initially, the particles form a circle (a), but as the wave passes into the page, space is stretched horizontally, and squeezed vertically (b). A half period later, however, the situation is reversed and space is squeezed horizontally and stretched vertically (d).*

address this question, Feynman, in characteristic style, anonymously proposed a simple thought experiment known as the "sticky bead" experiment. It goes as follows.

Consider a rod threaded through two rings as depicted in Fig. 2. The rings are allowed to slide along the rod, but there is some small friction between the rings and the rod. As a gravity wave traverses the experiment, space will get periodically stretched and compressed along the axis of the rod, meaning the proper-distance between the rings oscillates. On the other hand, the atomic restoring forces between the atoms in the rod will keep its length fixed. Consequently, the rings will rub against the rod, heating it. This implies that the gravitational wave is doing work on the system, and must therefore carry energy.

Also at the Chapel Hill conference was an engineer from the University of Maryland named Joseph Weber. He was fascinated by the phenomena of gravitational waves. So much so, that he went on to design the first experiment to directly detect them.

iii. Early Experimental Efforts

In the years following the Chapel Hill conference, Weber designed a ground based "antenna" which could detect the presence of gravity waves. He detailed his ideas in his 1960 paper "Detection and Generation of Gravity Waves"[8], and by 1966 had built a detector and published evidence of its performance[9].

Weber's experimental setup (see Fig. 3) consisted of a large aluminum cylinder, 66cm in diameter and 153cm in length[10]. The cylinder was suspended by

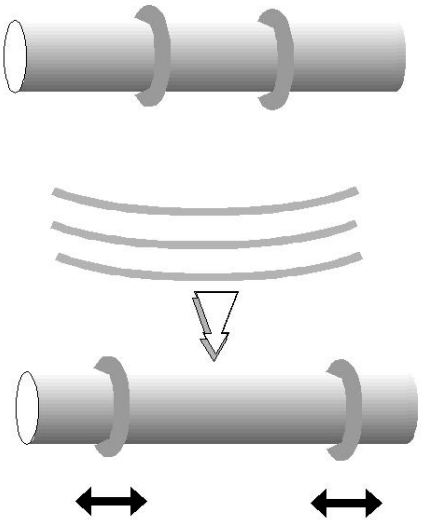

Figure 2: *Sketch of the "sticky bead" experiment.[7].*

steel wires from a vibration isolating support. Piezoelectric sensors were mounted around the diameter of the cylinder to detect vibrations, such as those induced by passing gravitational waves.

Weber actually built two of these detectors: one at the University of Maryland, and another nearly 1000 km away at Argonne National Laboratory outside Chicago, the idea being to use them to cross-check each other and eliminate false positives from local noise sources.

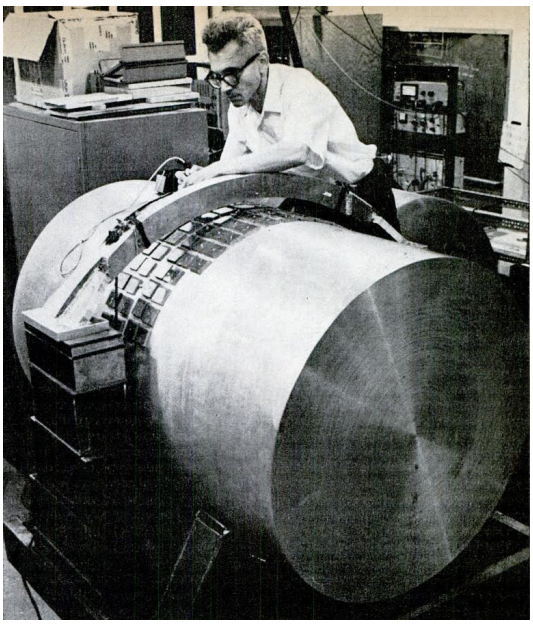

Figure 3: *Weber working on his detector*

Amazingly, when Weber turned on his detectors, they picked up about one coincidence a day (see Fig. 4). He claimed this as evidence for the discovery of gravity waves. He went further to claim that many of the signals originated near the center of our galaxy and estimated from his measurements that our galaxy is radiating $\approx$ 1000 solar masses per year of energy in the form of gravity waves. This ran afoul of estimates from cosmologists who calculated an upper limit of 200 solar masses per year. Any larger, and the necessary mass to hold the galaxy together would have radiated away long ago.

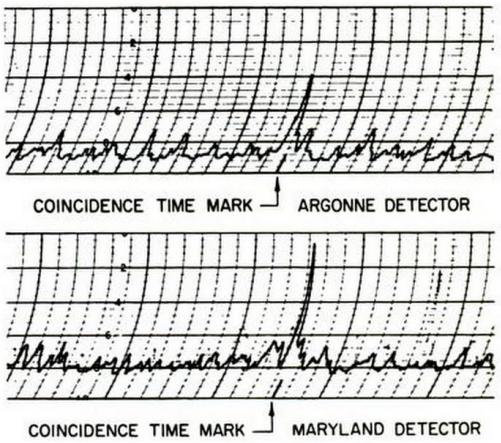

Figure 4: *An example of a detector coincidence seen by Weber published in the May 1972 issue of Popular Science*

A hallmark of all good science is repeatability. As such, efforts were undertaken by others to build similar resonating bar experiments to attempt to reproduce Weber's results. By the middle of the 1970s, several additional experiments were running that incorporated improvements over Weber's original design such as cooling the cylinders to reduce thermal noise. Sadly, none of these improved detectors were able to reproduce Weber's results. This inability to confirm Weber's results, combined with the unresolved disagreement with astronomic observations, convinced most members of the community that Weber's original observations were spurious.

With efforts at direct observation of gravity waves stymied for the moment, indirect observations would have to do. This came in the form of the observation of orbital decay in a binary pulsar system by Taylor and Hulse[11]. They used a 305 m diameter radio telescope to observe the electro-magnetic emissions of the pulsar over time and deduce changes in the relative distance between the earth and the pulsar over a period of several years. They then fit these measurements to a model to find the orbital period of the binary pulsar.

Their results[7] (including measurements made after their original publication in 1979) are shown in Fig. 5. As the pulsars orbit each other, they emit gravitational radiation which removes kinetic energy from the sys-

tem. As a result the orbital period decreases with time. This is precisely what was observed by Taylor et al. and their observations matched the predictions of General Relativity remarkably well.

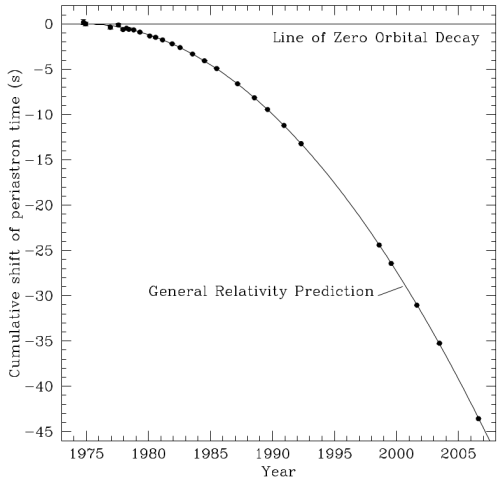

Figure 5: *The decay of the orbital period (labeled as periastron time) of PSR1913 due to the emission of gravity waves*

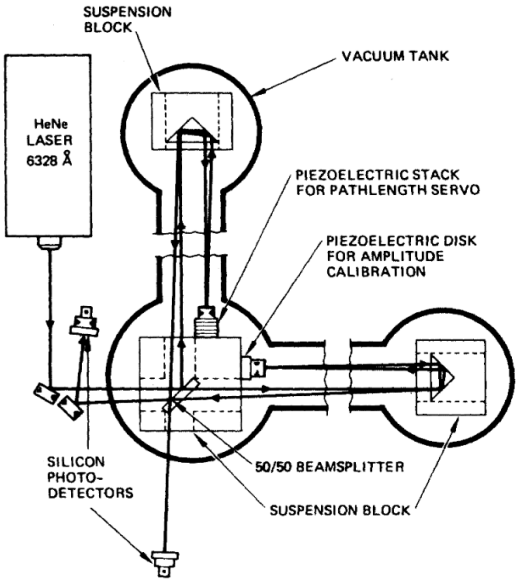

Figure 6: *A schematic of Robert Forward's early interferometer. Note the multiple paths the laser takes through each leg of the detector and the two photodetectors, used to mitigate electronic noise.*

iv. First Generation Interferometers

Given the lack of reproducible results from the Weber bar experiments, experimentalists began investigating completely different types of detectors for direct detection, the most promising of which was the laser interferometer. The earliest use of an interferometer to detect gravity waves was made by a former student of Weber named Robert Forward. Forward's detector (Fig. 6) consisted of 8.5 m arms and through 150 hours of observation found no coincidences with the Weber bar detectors simultaneously in operation[12].

The idea was not dead, however, and by the mid 1990s there were several large collaborations working on constructing long baseline interferometers. These included the GEO600 experiment in Germany, Virgo in Italy, and, most notably, LIGO in the United States.

The inception of what would eventually become LIGO happened in the summer of 1975 when Rainer Weiss, an experimentalist at MIT, and Kip Thorne, a theorist from Caltech, met at a conference hosted by NASA to explore the applications of space-based research to cosmology and relativity. As Thorne did not have a hotel room, he shared one with Weiss who recalls that night,

> "We made a huge map on a piece of paper of all the different areas in gravity. Where was there a future? Or what was the future, or the thing to do?"[13]

Inspired by his conversation with Weiss, Thorne decided that the thing to do at Caltech was to develop interferometers to detect gravity waves, and to accomplish this, he brought in an experienced experimentalist, Ronald Drever, to construct the detectors. For several years Weiss and Drever competed from opposite coasts to create better and better interferometers. Eventually, both groups came to the conclusion that a discovery sensitivity interferometer would have to be constructed at such a scale that attracting funding for separate experiments would be impossible. Therefore, with some prodding by the NSF, the Caltech and MIT groups joined forces and formed the "Laser Interferometer Gravitational-Wave Observatory" (LIGO).

Unfortunately, the triumvirate of Thorne, Weiss, and Drever proved unable to effectively manage the project so in 1986 the NSF instead appointed Rochus E. Vogt as the single project manager[14]. Despite this reshuffling of leadership, progress was slow. By 1994, Drever had left the project and Vogt was replaced with Barry Barish[2], a high-energy experimentalist who had experience working in large collaborations. Under Barish's leadership, the original plan for LIGO was reworked into a two-stage deployment. The first stage, named Initial LIGO, or iLIGO, would include the construction of two laboratories, one in Hanford, Washington, and the other in Livingston, Louisiana. They would be built with current generation interferometers that

[2]Born in Omaha, NE

would serve as a proof-of-concept and development platform for the second stage, known as Advanced LIGO. Advanced LIGO would use the same facilities as iLIGO, but replace the interferometers with next-generation designs.

Barish also suggested splitting the experiment into two separate entities. The first would be responsible for the administration and operation of the laboratory facilities, and the other, the "Ligo Scientific Collaboration", would be in charge of scientific and technological research, as well as forging alliances with other collaborations, most notably GEO600 and Virgo.

iLIGO began construction in 1995 and finished in 1997, however it still took until 2002 to begin taking scientific data, whereupon it operated in months-long runs across eight years before ceasing operation in 2010, having not yet observed gravity waves. This was not unexpected as the intention had always been to use iLIGO as a research and development platform to design Advanced LIGO, and the odds of actually making an observation with iLIGO were small.

III. The Advanced LIGO Detector

After the shutdown of iLIGO, efforts promptly began to install the upgraded systems of Advanced LIGO, and by February 2015[15], the experiments began taking "engineering mode" data to commission the new systems. Finally, in September of that year, it began taking scientific data.

i. Principle of Operation

An Advanced LIGO detector[16] is at its heart a Michelson style interferometer. This type of interferometer is displayed schematically in Fig. 7. The interferometer works by first producing a coherent light source, typically a laser, and then splitting the source into two beams that take different paths. The beams are then recombined and made to interfere with each other. The resulting interference pattern can then be used to infer the difference in the path lengths taken by the two lasers, or at least the distance modulo the wavelength of the laser.

If the two path lengths are exactly the same, the lasers will combine constructively and stimulate the sensitive element (a photo-diode) in the detector. However, as the path lengths diverge, the two beams will begin to interfere destructively and the resulting signal seen by the detector will decrease in amplitude until it disappears entirely when the path lengths differ by a half-wavelength.

In the case of LIGO, the nominal operating point is destructive interference at the detector, at the so-called "dark fringe". Accordingly, the detector end of the interferometer is referred to as the "dark port". As a gravity wave passes through the detector, it causes one leg of the detector to lengthen and the other to contract. This differential change in length appears as a departure from perfect destructive interference, and the larger the amplitude of the wave, the larger the signal seen by the photodetector.

It may be tempting to think that just as the space between the test masses (the splitter and the mirrors) gets stretched and squeezed with the passing of the gravity wave, so does the wavelength of the laser pulse, leading to no observable change in the interference pattern. It turns out that this is not the case. Although the laser's wavelength *does* get stretched and squeezed by the passing gravity wave, the effect is approximately ten-thousand times smaller than the effect on the test masses, well below the noise floor of LIGO. This is due to the fact that the spatial extent of LIGO ($\approx 4\,\text{km}$) is much smaller than the wavelength of the gravity waves being searched for ($\approx 3000\,\text{km}$).

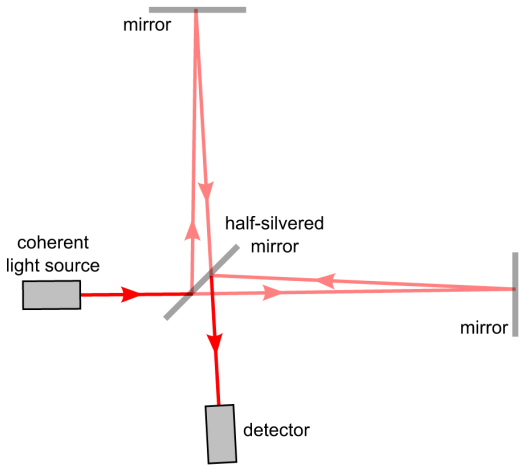

Figure 7: *Schematic representation of a Michelson interferometer.*

Unfortunately, a simple Michelson interferometer would not be sensitive enough to detect the tiny deformations from gravity waves. The limitation comes from the Michelson interferometer requiring a differential deformation on the order of λ to shift from fully-constructive to fully-destructive interference. A typical strain, defined as $h \equiv \frac{1}{2}\frac{\Delta l}{l}$, for the types of waves for which LIGO is searching is $h \approx 10^{-21}$ which gives a corresponding deformation of $4\,\text{km} * 10^{-21} = 4 \times 10^{-9}\,\text{nm}$ which is about 12 orders of magnitude smaller than λ. With such a large disparity, the resulting phase change would be too small to create a measurable deviation from the dark-fringe. Clearly, a way to get much larger phase shifts for a microscopic amount of deformation is needed.

The solution is the Fabry-Pèrot interferometer, or more precisely, owing to one end being almost a perfect mirror, the Gires-Tournois Interferometer[17]. In addition to the optical elements of the Michelson interferometer, this device adds an additional optical element in each leg between the beam splitter and the outer mirrors. The cavity formed by the new element and the outer mirror is tuned to be resonant with the incident laser. The Advanced LIGO setup is shown in Fig. 8.

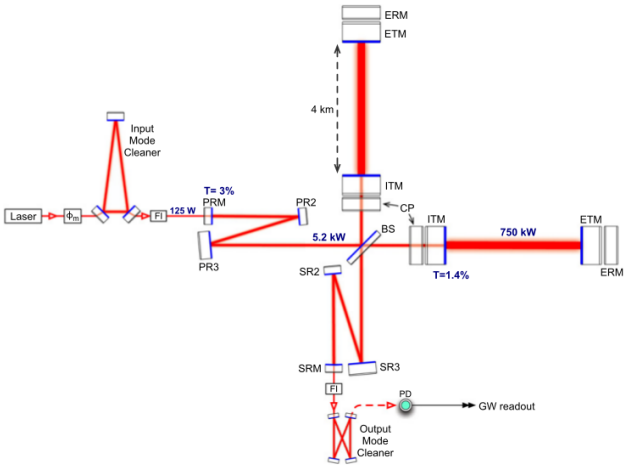

Figure 8: *The Advanced LIGO optical configuration.*

The Fabry-Pèrot resonant cavity in each leg is formed at one end by the end test mass (ETM) and at the other by the input test mass (ITM). The surface of the ETM is a nearly perfect mirror (failing to reflect only 5 ppm of the incident laser power), while the ITM has a reflection coefficient close to unity ($R = 98.6\%$). The phase for the returning beam is given by

$$\Phi = -2\tan^{-1}\left(\frac{1+\sqrt{R}}{1-\sqrt{R}}\tan\frac{\delta}{2}\right),$$

where

$$\delta \equiv \frac{4\pi}{\lambda} nL\cos\theta_L.$$

In the case of LIGO, n, the index of refraction in the chamber, is 1 since the laser is propagating through vacuum, λ, the wavelength of the laser is 1064 nm, and θ_L, the angle of refraction is zero as the laser is normally incident. Assuming these variables are well controlled, δ will depend only on L, the length of the resonant cavity.

If we now rewrite L in terms of the gravitational strain, h

$$L = L_0 + \Delta L = L_0(1+h),$$

we get

$$\delta = 4\pi\frac{4\,\text{km}}{1064\,\text{nm}}(1+h)$$

Strictly speaking, the above is only valid if thermal losses are small enough to be neglected. In reality, there are losses in the dielectric coatings of both the ETM and the ITM, but great care has been taken to make these losses small[3].

To illustrate how this improves the sensitivity of the detector for small values of h, Fig. 9 shows the phase shift as a function of strain for different internal reflectivities. Note that the $R = 0$ case corresponds to the normal Michelson interferometer where the ITM is transparent to the returning laser. As R tends towards unity, a more and more non-linear response appears due to increasing interference of the beam with itself after multiple traversals of the interferometer leg. This means that much better sensitivity to small h can be achieved by pushing R towards 1. Of consequence to the following discussion is the quantity known as *finesse*. It can be defined as

$$\mathcal{F}_c \equiv \frac{2\pi}{-\ln(R_1R_2)},$$

where R_1 and R_2 are the intensity reflectivities of the mirrors on either end of the Fabry-Pèrot cavity. In the previous example, $R_1 = 0.986$ and $R_2 = 1$ so the finesse of the LIGO arm cavities is about 445. Qualitatively, as the product of the reflectivities approaches unity, the finesse becomes large. In practice, the finesse is adjusted to balance the power stored in the cavity, and the sharpness of the transmission/reflection curves as a function of frequency (such a reflection curve is shown in Fig. 12).

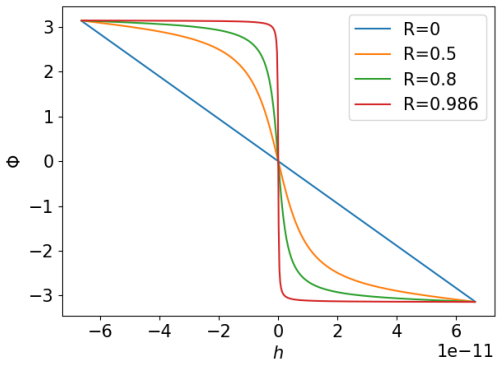

Figure 9: *Relations between the phase-shift, Φ, and h for various values of internal reflectivity R.*

[3]The drastically increased circulation power in Advanced LIGO, however, causes appreciable heating of the optics, leading to thermal lensing. Compensating heaters are added to the lenses to make their temperatures uniform throughout the bulk, mitigating this effect. The fractional losses are still small enough, however, to make the following calculations valid.

ii. The Laser and Input Optics

LIGO employs a multi-stage neodymium-doped yttrium aluminum garnet (Nd:YAG) laser that can supply up to 180 W of power to the interferometer. The laser source together with initial stabilizing and cleaning optics are referred to as the pre-stabilized laser (Fig. 11).

The laser cavity produces radiation with a nominal wavelength of 1064 nm, and frequency power distribution as shown in Fig. 10.

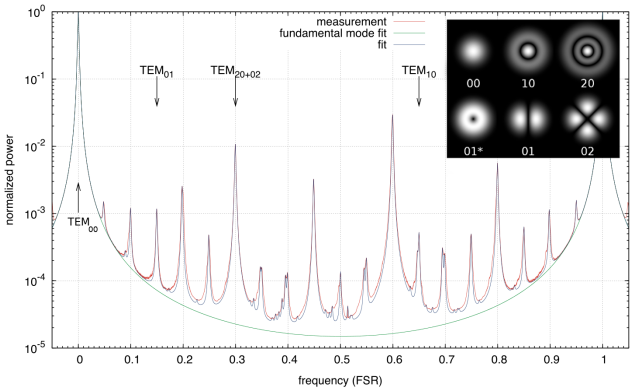

Figure 10: *Mode scan of the laser used at the Livingston Detector demonstrating that nearly 95 % of the laser's energy is in the* TEM_{00} *mode. The horizontal scale is in units of free spectral range (FSR) which is defined as* $\frac{c}{2L}$ *where L is the length of the resonant cavity. Inset: Intensity distributions of transverse laser modes for a cylindrically symmetric beam.*

To understand this figure, first note that the radiation produced by a laser cavity can be decomposed into transverse modes (see Fig. 10 inset). The presence of higher-order transverse modes in the beam is a problem because, due to the Gouy phase shift[4], the effective frequencies of these modes are higher than the frequency of the TEM_{00} mode. Since the interferometer is extremely sensitive to changes in laser frequency, it is therefore crucial to remove these other modes as much as possible. To that end, the beam is passed through the pre-mode-cleaner (PMC). This is a bow-tie (see Fig. 11) cavity that strips higher-order modes from the beam. For example, it reduces the amplitudes of the $\mathrm{TEM}_{01}/\mathrm{TEM}_{10}$ modes by a factor of 63. It also serves to provide low-pass filtering of RF intensity fluctuations.

After passing through the PMC, the beam goes through an RF modulator which adds low-amplitude phase modulation at 9 MHz, 45 MHz, and 24 MHz. The 9 and 45 MHz modulations are used for global sensing of the interferometer, while the 24 MHz modulation is used for input-mode-cleaner (IMC) sensing. These modulation side bands enable the use of the Pound-Drever-Hall[18] stabilization method. For a thorough description of the technique see [19]. Pound-Drever-Hall can be used for both laser frequency stabilization and Fabry-Pèrot cavity length stabilization. In fact, LIGO uses variations of the technique for both.

To illustrate the Pound-Drever-Hall method for laser frequency stabilization, consider a laser shining into a Fabry-Pèrot cavity with identical mirrors on either end. The laser is equipped with an actuator that can deform the lasing cavity to slightly alter the laser's frequency allowing for active correction of deviations from the ideal frequency. The transmission function of the cavity is given by

$$T_e = \frac{T^2}{1 + R^2 - 2R\cos\left(\frac{2L}{c}\left(\omega_0 + \Delta\omega\right)\right)} \quad ,$$

where R and T are the reflection and transmission coefficients of the cavity mirrors, L is the length of the cavity, ω_0 is the ideal, resonant, frequency in the cavity, and $\Delta\omega$ is a deviation from that ideal.

Of more interest for Pound-Drever-Hall is the reflectivity (Fig. 12) given simply by

$$R_e = 1 - T_e.$$

Now, a detector can be placed on the upstream side of the cavity to sense reflected light. If the detector sees anything, one can infer that the detector is off resonance, and the laser frequency has deviated from its ideal value[5]. Unfortunately, the error signal is symmetric about the resonance so the actuator in the lasing cavity does not know which way to adjust the laser to correct the error. Pound-Drever-Hall solves this by introducing a small phase modulation to the laser to operate the cavity slightly off resonance.

The modulated error signal then traces the reflection curve back and forth in the area highlighted by the inset of Fig. 12. If the frequency is too high, the error will trace up and down the curve on the right side of the minimum so the error signal will be in phase with the modulating signal, implying that the product of the error and modulation signal will be positive. On the other hand, if the frequency is too low, the signals will be half a period out of phase so the product will be negative. Therefore, by simply observing the sign of the product of the error signal and the modulating

[4] A phase shift resulting from the evolving interference of the plane waves that make up the beam.

[5] Note that this is in contrast with the LIGO arm cavities where the intensity of the reflected light is independent of laser frequency or arm length. In this case, the equation for T_e does not apply since the two ends have differing reflectivities. The applicable error signal in this case is the light shining into the dark port.

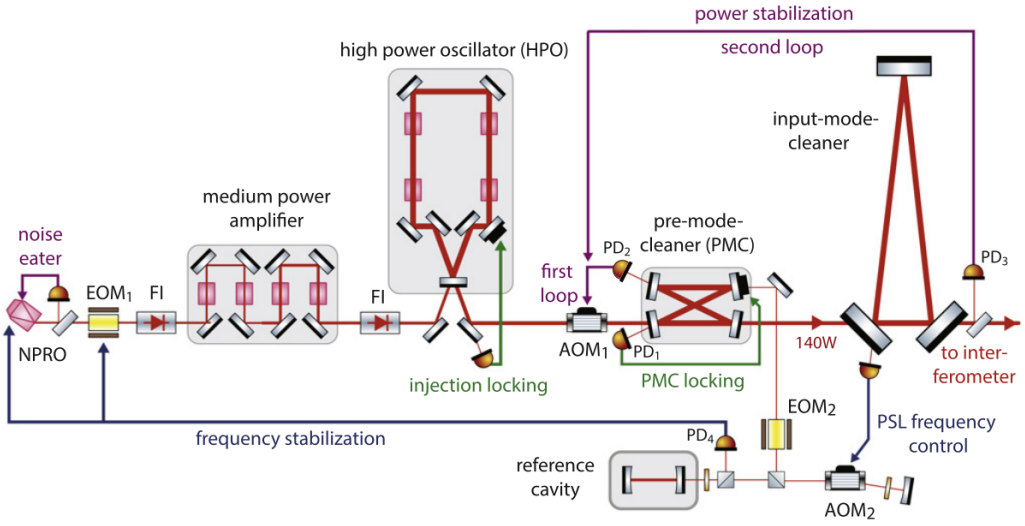

Figure 11: *Schematic of the pre-stabilized laser system. AOM: acousto-optic modulator, EOM: electro-optic modulator, FI: Faraday isolator, PD: photodetector, NPRO: non-planar ring-oscillator*

signal, the control system knows whether to adjust the frequency up or down.

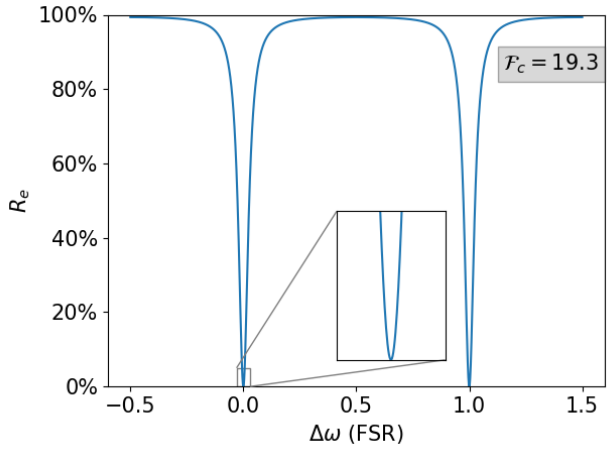

Figure 12: *The reflection coefficient of a Fabry-Pèrot cavity as a function of $\Delta\omega$, i.e. deviations in laser frequency.*

In a similar way, if the laser frequency is stable, but the length of the cavity is varying, the same scheme can be applied, with the only substantive difference being the actuator now applies a force to one or both of the cavity mirrors instead of the lasing cavity. This is the method used to keep all of the LIGO optical resonant cavities on their optimal working point.

After modulation, the beam passes through the final stage of the pre-stabilized laser system, the input-mode-cleaner. The input-mode-cleaner is used to further fix the laser's mode content, as well as stabilize the beam's position as it shines onto the power recycling mirror (PRM). Using the 24 MHz modulation and the Pound-Drever-Hall locking technique, it is able to help stabilize the frequency of the laser to $< 1 \times 10^{-3}\,\mathrm{Hz}/\sqrt{\mathrm{Hz}}$ at 100 Hz.

Finally, before being passed to the core optics of the interferometer, the beam passes through a Faraday Isolator which prevents light that is returning from the core optics from creating parasitic effects in the input chain.

iii. Core Optics

The output of the PSL is routed into the core interferometer optics. These consist of one ETM and one ITM for each leg. Adjacent to each ITM, there is also a compensation plate (CP) which is used as a reaction mass for actuating the ITM. Similarly, there is an end reaction mass for actuating the ETM.

The actuation of these optics is accomplished by applying a thin, circular, gold plating on the reaction masses that can be made to hold an electro-static charge by application of a voltage. This charge will push or pull on the dielectric test mass. The plating is divided into quadrants to also allow for aiming the test mass. iLIGO actually affixed magnets to the test masses and applied forces to the magnets via magnetic fields induced by coils mounted on the reaction masses. The electro-static method is preferred because mounting magnets on the test masses modifies their natural vibration modes, leading to additional thermal noise.

To round out the core optics, there is a 50/50 beamsplitter, four curved mirrors for signal (SR2, SR3) and

Optic	Diameter × thickness (cm)	Mass (kg)	Transmission	ROC (m)	Beam size (cm)
ITM	34 × 20	40	1.4% (0.5-2%)	1934	5.3
ETM	34 × 20	40	5 ppm (1-4%)	2245	6.2
CP	34 × 10	20	AR < 50 ppm	flat	5.3
ERM	34 × 13	26	AR < 1000 ppm	flat	6.2
BS	37 × 6	14	50%	flat	5.3
PR3	26.5 × 10	12	<15 ppm	36.0	5.4
SR3	26.5 × 10	12	<15 ppm	36.0	5.4
PR2	15 × 7.5	2.9	225 ppm (>90%)	-4.56	0.62
SR2	15 × 7.5	2.9	<15 ppm	-6.43	0.82
PRM	15 × 7.5	2.9	3.0%	-11.0	0.22
SRM	15 × 7.5	2.9	20%	-5.69	0.21

Table 1: *Parameters for the core optics. All transmission values are at* 1064 nm*, except for those in parentheses which are for* 532 nm*. AR: anti-reflection*

power (PR2, PR3) recycling, as well as the partially transmitting power recycling mirror (PRM) and signal recycling mirror (SRM). The integration of these elements into the LIGO architecture is shown in Fig. 8. Parameters for all these core optics, including dimensions, mass, transmission rates, radii-of-curvature, and beam size on the optic, are shown in Table 1.

One of the key improvements from iLIGO to Advanced LIGO was the addition of the signal recycling system. This can be seen in Fig. 8 as the elements SR2, SR3, and SRM. This serves to reshape the response of the interferometer to be more sensitive to signals in the low-audio frequency band that would come from binary neutron star or black hole coalescences[20]. The parameters of the signal recycling subsystem can be adjusted to enhance other frequency bands as well.

iv. Environmental Isolation

A great disadvantage of terrestrial experiments is that they are subject to the whims of nature, be it turbulent weather, the rumblings of the earth, or, in the case of the Livingston experiment, particularly heavy-footed alligators[6]. In fact, the ground motion at the sites of the two LIGO detectors is measured to be $\sim 10^{-6}\,\mathrm{m}/\sqrt{\mathrm{Hz}}$ while the perturbations from gravity waves are $\sim 10^{-18}\,\mathrm{m}/\sqrt{\mathrm{Hz}}$. This twelve order of magnitude difference emphasizes the importance, and the difficulty, of isolating the experiment from environmental vibrations.

The environmental isolation system is divided into two parts. The subsystem closest to the ground is referred to as the seismic isolation system, and the subsystem between that and the test masses is the suspension system. As shown in Fig. 16, these systems reduce the effects of ground motion to less than $10^{-20}\,\mathrm{m}/\sqrt{\mathrm{Hz}}$ at 100 Hz.

[6] not measurable

The seismic isolation system, shown in some detail in Fig. 14, consists first of the Hydraulic External Pre-Isolator (HEPI) system that uses a blend of geophones and inductive position sensors together with hydraulic actuators to damp low frequency (0.1 Hz-10 Hz) vibrations. This supports the Internal Seismic Isolation (ISI) system. The ISI sits inside vacuum and consists of three stages (labeled in the figure as Stage 0, Stage 1, and Stage 2) that are sequentially suspended and sprung from each other. The stages are instrumented with capacitive position sensors and controlled with electromagnetic force actuators. The stage 2 structure includes an optics table from which the optical elements are suspended.

All of the in-vacuum core optics are mounted on elaborate multi-stage suspension systems of various designs based on noise requirements. Table 2 lists these noise requirements along with number of spring-based vertical isolation stages, pendulum stages, and suspension wire types. An example of all of these things put together, in this case for the ITM, is shown in Fig. 13.

A pendulum suspension is a wonderful choice for passive filtering of environmental vibrations due to the property that above its resonance frequency, it suppresses noise by a factor of ω^{-2}. And this property can be chained by hanging pendula from other pendula. For the test masses, there are four pendula stages, yielding filtering $\propto \omega^{-8}$ for ω greater than all the resonance frequencies of the system. Unfortunately, this only serves to damp horizontal motion, and, although horizontal noise in the test masses causes the most direct damage to signal quality, vertical and angular misalignment also contribute. To provide for isolation from vertical noise, cantilevered spring stages are employed both in the suspension and in the seismic isolation systems.

Optical component	Vertical iso. stages	Pendulum stages	Final stage fibre type	Longitudinal noise requirement @ 10 Hz (m/$\sqrt{\text{Hz}}$)
Test masses (ITM, ETM)	3	4	Fused silica	1×10^{-19}
Beamsplitter (BS)	2	3	Steel wire	6×10^{-18}
Recycling cavity optics	2	3	Steel wire	1×10^{-17}
Input mode cleaner (IMC) optics	2	3	Steel wire	3×10^{-15}
Output mode cleaner (OMC) assembly	2	2	Steel wire	1×10^{-13}
ETM transmission monitor	2	2	Steel wire	2×10^{-12}

Table 2: *Suspension parameters for the core optics.*

IV. Signal Extraction

The raw signal coming from the photo-diodes at the dark port are unsuitable for direct analysis because it contains a convolution of the gravity wave strain with the detector's response. The gravity wave signal, h, is proportional to the differential length change, $\Delta L_{\text{free}} = L_x - L_y = hL$, where $L \equiv (L_x + Ly)/2$ is the average arm length. By rearranging the equation, we get $h = \Delta L_{\text{free}}/L$. Now, the control system of LIGO does not actually allow for the lengths to change freely. Instead, it actuates the test masses to compensate for the strain and always tries to keep the differential arm length at zero. Therefore, the "free" displacement, ΔL_{free}, will be reduced to a residual length change defined by the response of the detector,

$$\Delta L_{\text{res}} = \frac{\Delta L_{\text{free}}}{1 + G(f)}.$$

The detector response function, $G(f)$, is further broken down into three components: the sensing function $C(f)$, the digital filter function $D(f)$, and the actuation function $A(f)$. Together, these give the open loop transfer function

$$G(f) = A(f)D(f)C(f).$$

Fig. 15 shows a block diagram describing the control and calibration system. For a detailed description of how these functions are modeled and calibrated, see [21]. Suffice to say here that once $G(f)$ is known, ΔL_{res} can be used to find ΔL_{free}, which in turn can be used to calculate the gravitational strain h.

One of the key performance metrics of a gravity wave interferometer is the detector noise in the frequency band of interest. For LIGO, this band is approximately 20Hz to 1000Hz, with peak design sensitivity around 100 Hz. Fig. 16 shows the spectral density of the noise in the Advanced LIGO detector. Lower val-

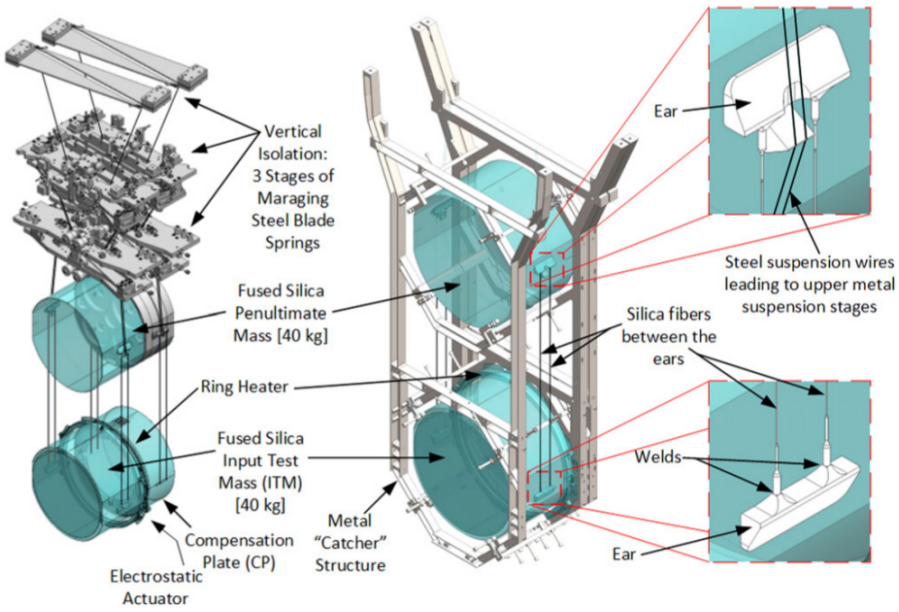

Figure 13: *Illustration of the suspension system for the ITM showing the three vertical isolation stages and four pendulum stages. The center image shows the so-called "earthquake-stop", also known as the catcher structure.*

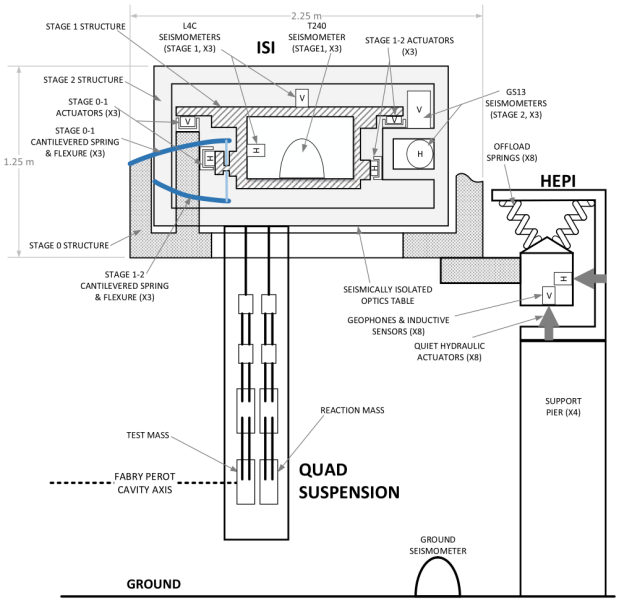

Figure 14: *Schematic of the seismic isolation system for the test mass optics.*

ues here lead directly to higher sensitivities to gravity wave signals. The various peaks in the distributions come from calibration lines (33-38, 330, and 1080 Hz), the harmonic modes of optic suspension fibers (500 Hz and harmonics), and harmonics of the 60 Hz power line. The dominant contributor to noise at high frequencies is the quantum, or *shot*, noise which comes from the uncertainty in the arrival times of photons to the photodetector. This translates to a Poisson distribution of the number of photons detected in a given time interval. The shorter the interval, the larger the relative uncertainty in the number of photons, going

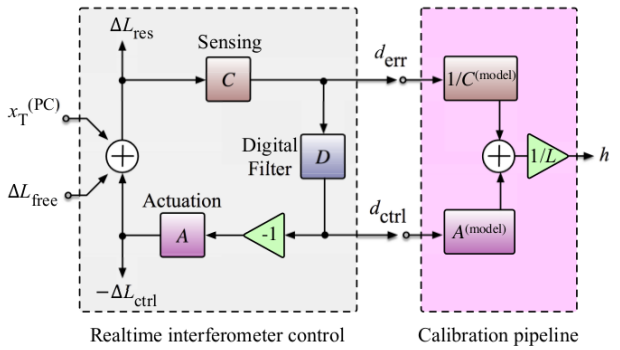

Figure 15: *The sensing and control feedback loop of LIGO. $x_T^{(PC)}$ is a calibration displacement caused by an auxiliary laser source exerting pressure on the test masses.*

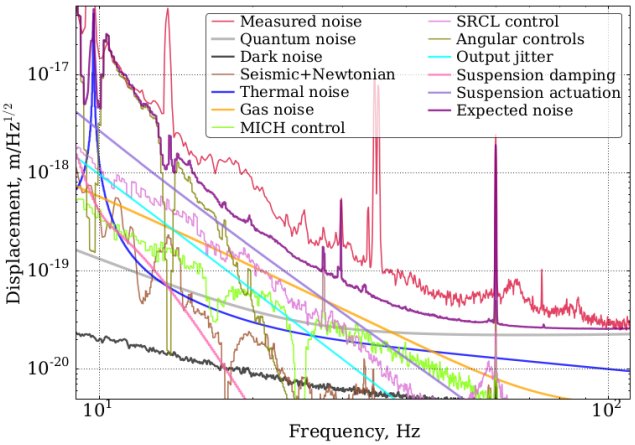

(a) Low frequency noise at the Livingston Observatory

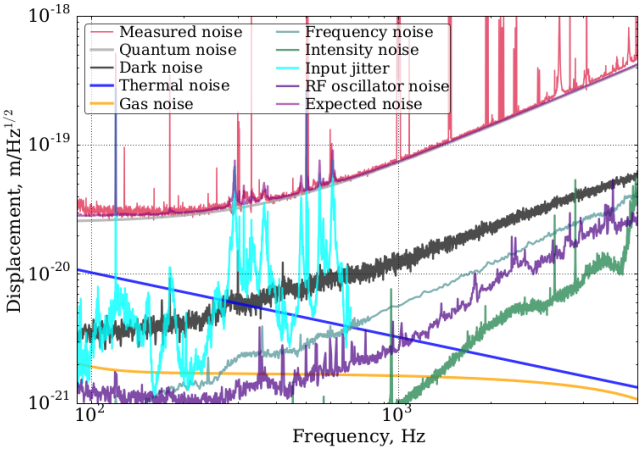

(b) High frequency noise at the Hanford Observatory

Figure 16: *The noise budget plots for the gravitational wave channels of the two LIGO detectors. The sensitivities are similar for both sites.*

as

$$\frac{\sigma}{\hat{N}} \propto \frac{1}{\sqrt{\Delta t}} = \sqrt{f}.$$

At low frequencies, the main noise contributions are due to residual seismic vibrations. For a full description of the different noise sources shown in Fig. 16, see [22].

V. Observations

Once $h(t)$ is known, it is possible to begin to search for signatures of gravity waves for a variety of sources, including asymmetric pulsars, supernovae, and primordial gravity waves from the big-bang. But the most likely to be seen is from inspirals and mergers of binary systems composed of neutron stars or black holes. So far, the two events that have been identified by LIGO are both binary black hole mergers. The signature of these events is illustrated in Fig. 17. Note the

three distinct stages of the signature. The earliest is when the black holes are still well separated compared to their Schwarzschild radii, but their mutual orbits emit gravitational radiation. The frequency and amplitude of the radiation gradually ramp up as the black holes' orbits become tighter and tighter. Eventually, the black holes get close enough that they merge. This is a violent, highly non-linear process that requires precise numerical simulations to accurately predict. Finally, there is the "ring-down" phase where the final black hole radiates away all of its leftover inhomogeneities, or "hairs", to reach its stable state where it is defined only by its mass and spin.

The primary technique used to find incidents of binary black hole mergers in the data stream from LIGO is matched filtering. This technique works by first generating a simulated waveform and then convolving that with the data in the time domain to find peaks which indicate a match. This is a bit like printing the pattern on a piece of transparency and then sliding the pattern along the data stream until the data and the pattern line up. One issue, of course, is that there is a huge sensitivity to small errors in frequency since just a single half-wavelength deviation would cause a negative contribution to the convolution even though the pattern may be, at least to the eye, a good match. As such, great pains have been taken to produce accurate and plentiful simulations of black hole mergers throughout the parameter space defined by differing masses, spins, and orientations. Overall, approximately 250 000 signal waveforms were generated and simultaneously tested against the LIGO data stream in parallel using supercomputing facilities[1]. Both LIGO sites run the matched filtering search independently to search for candidate events. They then compare their candidates to find events consistent with the 10 ms inter-site propagation time (Fig. 18).

To determine the statistical significance of the matched events, background estimation is done using a time-shift method. This method artificially shifts the timestamps of one detector's data by a large amount compared to the inter-site propagation time, thereby decorrelating any real events in the data. A new set of events is then calculated from this data that are purely the result of detector noise conspiring to make something that looks like a real event. This procedure can be repeated many times for different time offsets to produce the equivalent of 608 000 years of background-only data. From this, estimates of the number of fake events reaching various significances can be extracted. Since this "background" sample in reality contains a mixture of background and signal, it will produce an overestimate of the number of background events with a given significance since a real event correlated

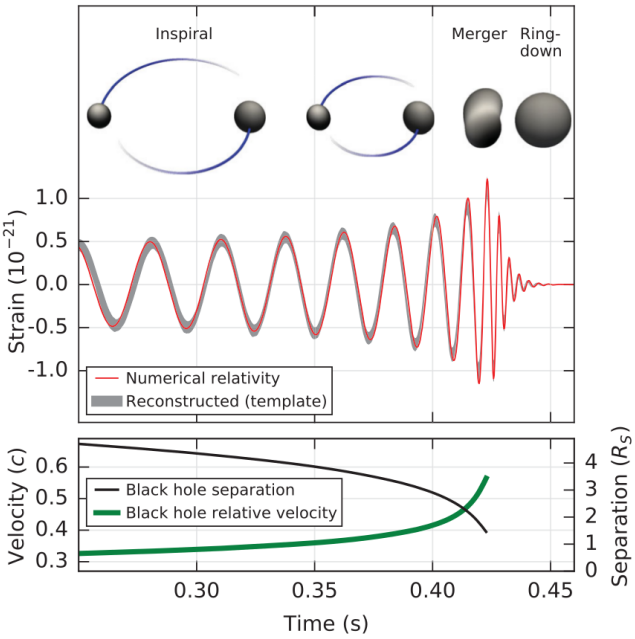

Figure 17: *(top) The three stages of binary black hole coalescence. (middle) The matching waveform that was used to detect GW150914, and (bottom) the relative velocity determined from the parameter* $\frac{v}{c} = \left(GM\pi f/c^3\right)^{1/3}$, *and the separation in units of Schwarzschild radius* $R_s = 2GM/c^2$.

with noise will be more significant than noise correlated with noise. Therefore, the procedure was repeated with events confidently identified as being real removed. The results of this analysis for the event GW150914 are shown in Fig. 19. Note the good agreement between the number of expected and detected low-significance events down to approximately one event predicted, and the well separated signal event. Most of the high-significance background events were caused by GW150914 correlating with noise from the other detector. With that event removed, the number of high-significance background events drops appreciably (purple line).

In the first Advanced LIGO science run, which started on September 12, 2015 and concluded on January 19, 2016, the experiment identified two gravity wave events: GW150914, and GW151226. The key demographics for these events are shown in Table 3. The source of each event can be mapped to the sky based on the time delta of the signal between the two detectors with some additional information provided by the amplitudes and phases. Sky-maps for both events are shown in Fig. 20.

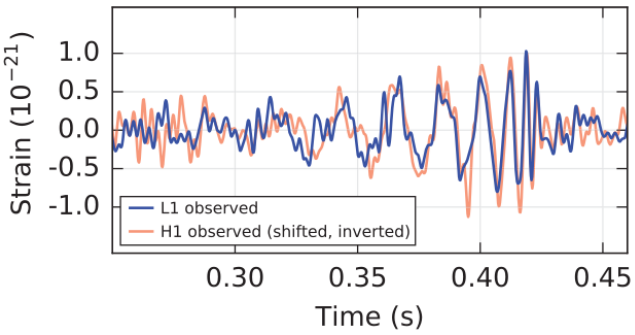

Figure 18: *The matched strain data from the Livingston (L1) and Hanford (H1) detectors for event GW150914. For visualization, the waveform has been processed with a 35-350*Hz *bandpass filter to remove large fluctuations outside the detector's most sensitive band as well as band-reject filters to remove the strong instrumental spectral lines seen in Fig. 16.*

	GW150914	GW151226
Primary mass $m_1/M_\odot$	$36.2^{+5.2}_{-3.8}$	$14.2^{+8.3}_{-3.7}$
Secondary mass $m_2/M_\odot$	$29.1^{+3.7}_{-4.4}$	$7.5^{+2.3}_{-2.3}$
Radiated energy $E_{rad}/M_\odot$	$3.0^{+0.5}_{-0.4}$	$1.0^{+0.1}_{-0.2}$
Luminosity distance D_L/Mpc	420^{+150}_{-180}	440^{+180}_{-190}
Source redshift z	$0.09^{+0.03}_{-0.04}$	$0.09^{+0.03}_{-0.04}$
Sky localization $\Delta\Omega$/ deg^2	230	850

Table 3: *Physical attributes of the two black hole merger events seen in Advanced LIGO's first science run.* $M_\odot$*: one solar mass,* Mpc*: megaparsec or approximately three million light-years*

VI. Astrophysical Implications

The observation of gravity waves was a wonderful confirmation of the predictions of general relativity, but there are additional implications to cosmology and other areas of physics.

With regards to cosmology, the observations of LIGO are confirmation that binary black hole systems are created and can coalesce on the timescale of the age of the Universe. Given the measured event rate and estimated detector efficiency, the rate of binary black hole coalescences is estimated at $55^{+103}_{-41}\mathrm{Gpc}^{-3}\,\mathrm{yr}^{-1}$. Going further, estimates can be made on the mass distribution of binary black holes. Using a power-law model,

$$p(m_1) \propto m_1^{-\alpha}$$

where $5M_\odot \leq m_2 \leq m_1$ and $m_1 + m_2 \leq 100M_\odot$, one can infer based on the observed events that $\alpha = 2.5^{+1.5}_{-1.6}$. Both of these estimates may be somewhat premature, hence the large error bars, but they will both become more precise as more data is collected. Regardless, the observed events demonstrate the existence of stellar-mass black holes more massive than $\simeq 25M_\odot$.

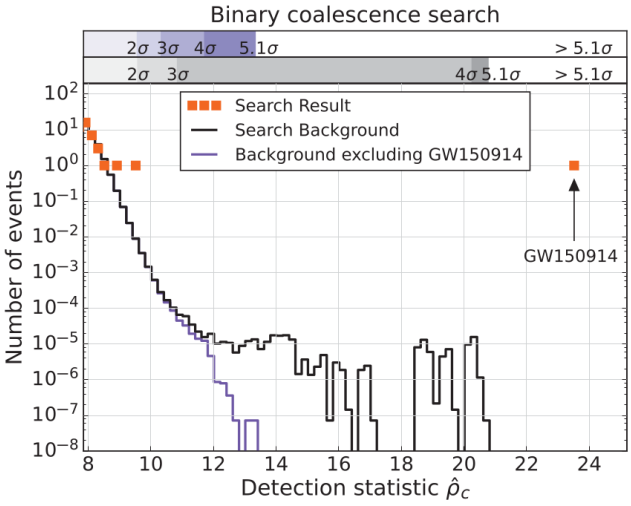

Figure 19: *Significance of event GW150914. Lines show the number of background events with the specified detection statistic estimated from the time-shifted data. Boxes show the number of measured events.*

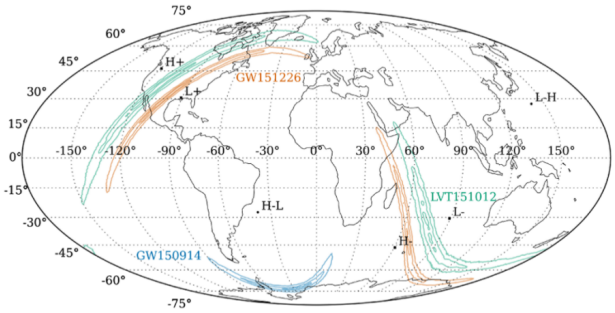

Figure 20: *Probability distributions for the sky locations of GW150914, GW151226, as well as the less significant LVT151012 which is not discussed in this paper.*

The graviton is the postulated mediator for the gravitational force. If it exists, it should have zero mass due to the apparent infinite range of the gravitational force and an intrinsic spin of $2\hbar$, since it arises from the rank-2 stress-energy tensor. The observation of gravity waves is in no way evidence for gravitons, but if one postulates their existence, certain bounds on their properties can be extracted from the observed events. Specifically, the dispersion of the wave as it propagates through space can yield information on the graviton's Compton wavelength and hence its mass. Doing this gives an upper bound on the graviton's mass of $1.2 \times 10^{-22}\,\mathrm{eV\,c^{-2}}$[23].

Evidence for the spin-2 nature of the graviton exists in the wave polarizations ($+$ and $\times$). The current pair

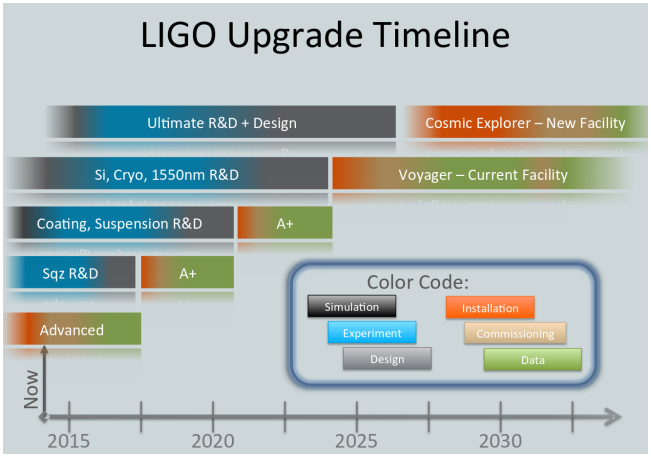

Figure 21: *Timelines for "A+", Voyager, and Cosmic Explorer facilities*

of LIGO observatories are roughly aligned with each other so they see very similar linear combinations of the two modes, making it infeasible to decompose the detected gravity wave into polarizations.

VII. Outlook & Conclusions

In this paper I have discussed many aspects of the Advanced LIGO experiment, and hopefully conveyed a sense of the scientific and technological achievement of the experiment. But this is just the beginning. As more observatories are set to come online in the coming decade, including Advanced Virgo, and LIGO India, sensitivities and sky-map localization will improve dramatically. Other proposed detectors include LISA, a space-based interferometer specializing in longer period gravity waves. These could arise from sources such as super-massive black hole coalescences from galactic mergers, or stellar-mass black holes falling into a super-massive black hole.

For LIGO itself, there are a variety of "A+" proposals that cumulatively would double Advanced LIGO's sensitivity and range. These would be retrofitted to the existing detector over the next decade and include using "squeezed light" to decrease the radiation-pressure and shot noise as well as improving the optical coatings to reduce mechanical losses[24]. Projecting further into the future, there are also proposals for an upgraded interferometer installed in the current LIGO facilities called LIGO *Voyager*, as well as an entirely new facility called LIGO *Cosmic Explorer*. The timelines for these proposed facilities are shown in Fig. 21.

The observation of gravity waves was a great moment in scientific history, and the future of the nascent field of gravity wave astronomy is bright. With hard work and bit of luck, many great discoveries lie in the future.

Author's note: Shortly after the writing of this paper, the LIGO Scientific Collaboration announced a third detection of a binary black hole system designated as GW170104[25]. The event was reconstructed with a total mass of $50M_{\odot}$. The new data updates the coelescence rate to $103^{+110}_{-63}\mathrm{Gpc}^{-3}\,\mathrm{yr}^{-1}$, and the m_1 mass distribution parameter, α, to $2.3^{+1.3}_{-1.4}$.

References

[1] The LIGO Scientific Collaboration. Observation of Gravitational Waves from a Binary Black Hole Merger. *Phys. Rev. Lett.*, 116:061 102, Feb 2016. doi:10.1103/PhysRevLett.116.061102.

[2] The LIGO Scientific Collaboration. GW151226: Observation of Gravitational Waves from a 22-Solar-Mass Binary Black Hole Coalescence. *Phys. Rev. Lett.*, 116:241 103, Jun 2016. doi:10.1103/PhysRevLett.116.241103.

[3] Poincare, H. Sur la Dynamique de l'èlectron. *Proc. Acad. Sci.*, 140:1504–1508, 1905. In French.

[4] Einstein, A. Integration Näherungsweise Feldgleichungen der der Gravitation. *Sitzungsber. Preuss. Akad. Wiss. Berlin (Math.Phys.)*, 22:688–698, 1916. In German.

[5] Pirani, F.A.E. Republication of: On the physical significance of the Riemann tensor. *General Relativity and Gravitation*, 41(5):1215–1232, 2009. ISSN 1572-9532. doi:10.1007/s10714-009-0787-9.
URL `http://dx.doi.org/10.1007/s10714-009-0787-9`

[6] Thorne, K. Caltech Physics 237 course notes. online.
URL `http://elmer.tapir.caltech.edu/ph237/`

[7] Cervantes-Cota, J.L., *et al.* A Brief History of Gravitational Waves. *Universe*, 2(3), 2016. ISSN 2218-1997. doi:10.3390/universe2030022.
URL `http://www.mdpi.com/2218-1997/2/3/22`

[8] Weber, J. The Detection and Generation of Gravity Waves. *Physical Review*, 117:306–313, 1960.

[9] Weber, J. Observation of the Thermal Fluctuations of a Gravitational-Wave Detector. *Physical Review Letters*, 17:1228–1230, 1966.

[10] Weber, J. How I Discovered Gravitational Waves. *Popular Science*, pages 106–107,190–192, May 1972.

[11] Taylor, J.H., *et al.* Measurements of general relativistic effects in the binary pulsar PSR1913 + 16. *Nature*, February 1979. doi:10.1038/277437a0.

[12] Forward, R. Wide band Laser-Interferometer Gravitational-radiation experiment. *Phys. Rev. D*, 17:379–390, 1978.

[13] Janna, L. *Black Hole Blues and Other Songs from Outer Space*. Knopf, New York, NY, USA, 2016.

[14] Russel, R. Catching the wave. *Sci. Am.*, 266:90–99, 1992.

[15] Davide, C. Hunt for gravitational waves to resume after massive upgrade: LIGO experiment now has chance of detecting ripples in space-time. *Nature*, 525:301–302, 2015.

[16] The LIGO Scientific Collaboration. Advanced LIGO. *Classical and Quantum Gravity*, 32(7):074 001, 2015.
URL `http://stacks.iop.org/0264-9381/32/i=7/a=074001`

[17] F., G. and P., T. Interferometre utilisable pour la compression d'impulsions lumineuses modulees en frequence. *C. R. Acad. Sci. Paris*, 258:6112–6115, Feb 1964.

[18] Drever, R.W.P., *et al.* Laser Phase and Frequency Stabilization using an Optical Resonator. *Appl. Phys. B*, 31:97–105, 1983.

[19] Black, E.D. An introduction to Pound-Drever-Hall laser frequency stabilization. *Am. J. Phys.*, 69:97–105, January 2001.

[20] Meers, B.J. Recycling in laser-interferometric gravitational-wave detectors. *Phys. Rev. D*, 38(8):2317–2326, October 1988.

[21] The LIGO Scientific Collaboration. Calibration of the Advanced LIGO detectors for the discovery of the binary black-hole merger GW150914. *Phys. Rev. D*, 95:062 003, Mar 2017. doi:10.1103/PhysRevD.95.062003.
URL `https://link.aps.org/doi/10.1103/PhysRevD.95.062003`

[22] Martynov, D.V., *et al.* Sensitivity of the Advanced LIGO detectors at the beginning of gravitational wave astronomy. *Phys. Rev. D*, 93:112 004, Jun 2016. doi:10.1103/PhysRevD.93.112004.
URL `https://link.aps.org/doi/10.1103/PhysRevD.93.112004`

[23] Abbott, B.P., *et al.* Tests of General Relativity with GW150914. *Phys. Rev. Lett.*, 116:221 101, May 2016. doi:10.1103/PhysRevLett.116.221101.
URL `https://link.aps.org/doi/10.1103/PhysRevLett.116.221101`

[24] McClelland, D., *et al.* Instrument Science White Paper 2015. Technical report, LIGO Scientific Collaboration, July 2016.
URL `https://dcc.ligo.org/LIGO-T1500290/public`

[25] LIGO Scientific and Virgo Collaboration. GW170104: Observation of a 50-Solar-Mass Binary Black Hole Coalescence at Redshift 0.2. *Phys. Rev. Lett.*, 118:221 101, Jun 2017. doi:10.1103/PhysRevLett.118.221101.
URL `https://link.aps.org/doi/10.1103/PhysRevLett.118.221101`